ARTICLE   OPEN

Check for updates

Antigen self-anchoring onto bacteriophage T5 capsid-like particles for vaccine design

Emeline Vernhes [1,5], Linda Larbi Chérif[2,5], Nicolas Ducrot [1], Clément Vanbergue[2], Malika Ouldali[1], Lena Zig[2], N'diaye Sidibe[2], Sylviane Hoos[3], Luis Ramirez-Chamorro[1], Madalena Renouard[1], Ombeline Rossier [1], Patrick England [3], Guy Schoehn [4], Pascale Boulanger [1 ✉] and Karim Benihoud[2 ✉]

The promises of vaccines based on virus-like particles stimulate demand for universal non-infectious virus-like platforms that can be efficiently grafted with large antigens. Here, we harnessed the modularity and extreme affinity of the decoration protein pb10 for the capsid of bacteriophage T5. SPR experiments demonstrated that pb10 fused to mCherry or to the model antigen ovalbumin (Ova) retained picomolar affinity for DNA-free T5 capsid-like particles (T5-CLPs), while cryo-EM studies attested to the full occupancy of the 120 capsid binding sites. Mice immunization with CLP-bound pb10-Ova chimeras elicited strong long-lasting anti-Ova humoral responses involving a large panel of isotypes, as well as CD8+ T cell responses, without any extrinsic adjuvant. Therefore, T5-CLP constitutes a unique DNA-free bacteriophage capsid able to display a regular array of large antigens through highly efficient chemical-free anchoring. Its ability to elicit robust immune responses paves the way for further development of this novel vaccination platform.

INTRODUCTION

Tackling infectious endemic diseases and emerging pandemics requires new vaccines providing maximum safety, tolerability and immunogenicity. Virus-Like Particles (VLPs) offer great potential for targeted antigen (Ag) delivery and meet these requirements. They self-assemble into non-infectious particles mimicking the real virus and constitute multivalent Ag-display platforms. Their nanoscale size combined with the multimerization of the Ag on their repetitive surface geometry play a major role in their ability to trigger potent immune responses[1–3]. Currently licensed VLP-based vaccines targeting Human Papillomavirus (HPV)[4] or Hepatitis B virus (HBV)[5] rely on viral proteins carrying their own Ag. Yet, the need to diversify VLP-vaccines open the quest for universal virus-like scaffolds able to display heterologous Ags. Viruses infecting bacteria, or bacteriophages, have been proposed as versatile and efficient Ag-nanocarriers for mounting immune responses against different Ags[6]. Most of them enclose their genome in an icosahedral capsid that constitutes a highly stable platform for Ag-display. During the last decade, several infectious phage particles were used for vaccination assays against human pathogens in murine models[7]. Among them, bacteriophage T4 was engineered by grafting Ags to the capsid surface or by modifying the phage genome to deliver DNA encoding Ags from *Y. pestis*[8] or more recently SARS-CoV-2[9]. While infectious phages are often easier to produce than their genome-free capsid, their use as vaccines in human clinical trials is confronted to international regulatory issues posed by the use of self-replicating viruses in medicine, as is currently the case with phage therapy[10]. In contrast, phage capsids devoid of viral genome could meet regulatory requirements applicable to VLPs. VLPs derived from RNA phages self-assemble upon expression of the gene encoding their coat protein (CP). The CP can tolerate the genetic fusion of Ag to its N- or C-terminal ends or insertion in external unstructured loops[11]. However, the self-assembly of Ag-VLP based on genetic fusion is limited to relatively small Ags (<50 amino acids)[12], or can be achieved if only a small proportion of CP subunits bears larger Ags[13]. Chemical crosslinking or bio-conjugation technologies, like SpyTag/SpyCatcher conjugation that creates a covalent iso-peptide bond between pre-purified VLPs and Ags, were used to overcome this limitation. However, the Ag-coupling efficiency is highly variable and difficult to control, ranging from 20 to 80% depending on the Ag[14,15]. Capsid decoration proteins that are found in some tailed bacteriophages constitute an attractive alternative to conjugation methods. These proteins spontaneously attach to their specific sites onto the mature capsid once the genome has been packaged and represent potential home bases for Ag display. The decoration protein gpD of phage Lambda, which binds as trimer spikes to the three-fold axes of the capsid, was genetically or chemically modified to display heterologous Ag on self-assembled VLPs derived from Lambda capsid[16]. Although these VLPs have proven to elicit strong humoral immune responses in mice[17], the methods used for Ag grafting do not allow full Ag load. Further development of phage capsids for vaccination requires reliable scaffolds that can efficiently anchor Ags in a precise array independently of their sizes. With this in mind, we turned our interest toward the large icosahedral capsid from bacteriophage T5 (90 nm in diameter)[18]. The capsid shell is formed of 775 subunits of the CP (the major capsid protein pb8) organized as hexamers on the faces and pentamers on 11 of the 12 vertices[19]. Its outer surface displays a monomeric decoration protein pb10 (17.3 kDa) bound at the center of each of the 120 CP hexamers[19]. pb10 is formed of an N-terminal capsid-binding domain (pN), connected by a flexible linker to a C-terminal immunoglobulin (Ig)-like domain (pC) exposed to the solvent (Fig. 1a). The pN domain alone anchors with the same high affinity as full-length pb10 to its binding sites ($K_D = 10^{-12}$ M), while the pC domain does not interact
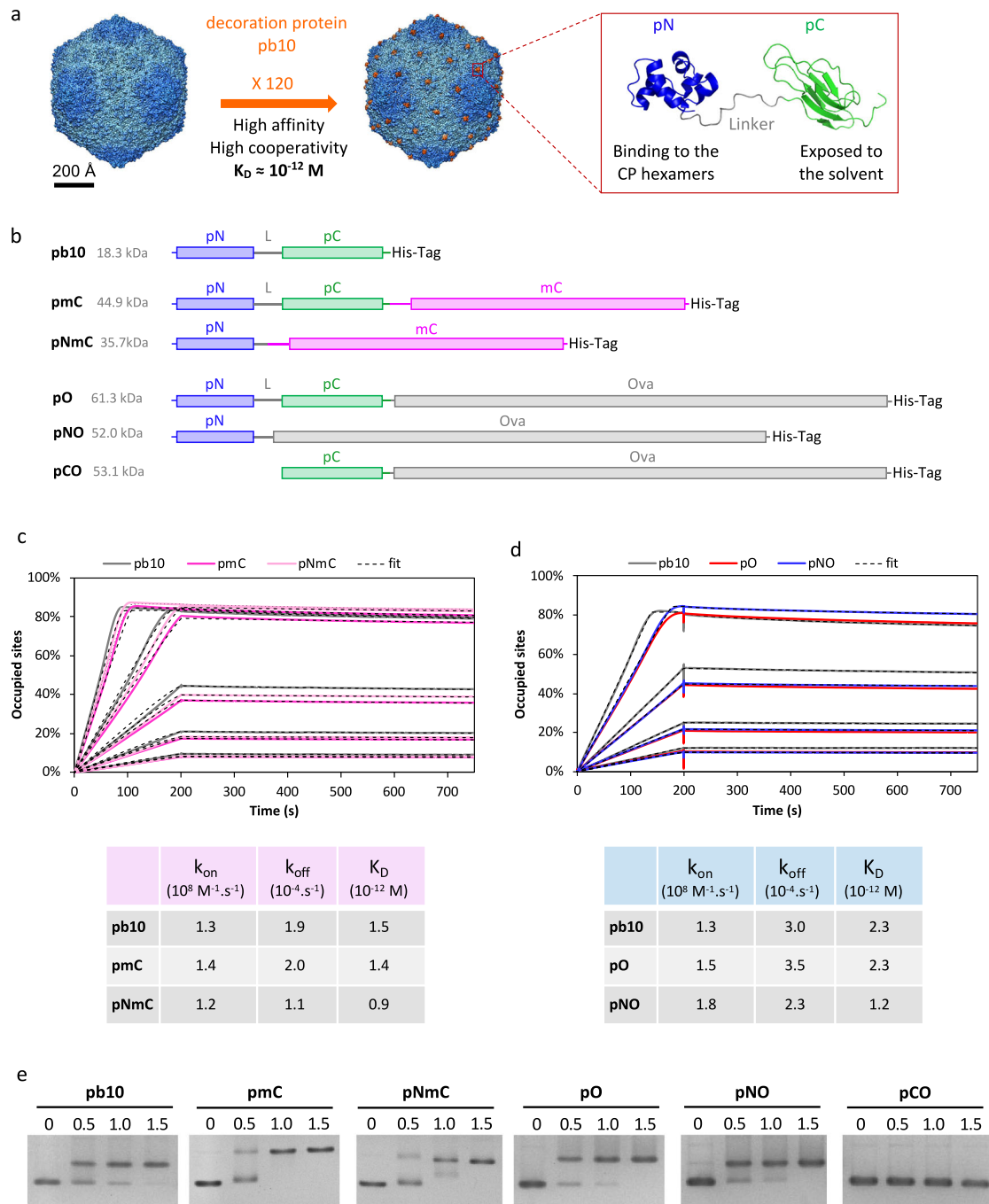
Fig. 1 Anchoring of pb10-chimeras onto T5 CLPs with picomolar affinity. a High-affinity decoration of T5 capsid with 120 copies of the protein pb10, as seen on the surface view of T5 capsid density maps (represented from EMDB accession codes 6OMA and 6OMC). The backbone structure of pb10 shows the capsid anchoring N-terminal domain pN (blue, PDB code 5LXL) and the C-terminal domain pC (green, PDB code 5LXK). **b** Schematic representation of pb10-chimeras pmC, pNmC, pO, pNO and pCO used in this study, with reference to the native protein pb10. The N-terminal (pN) and C-terminal (pC) domains of pb10 are in blue and green respectively. L is the linker region between pN and pC domains. The fused heterologous proteins mCherry (mC) and Ovalbumin (O) are in pink and gray, respectively. The lines represent the unfolded flexible regions while the rectangles represent the structured domains of each protein. **c, d** SPR real-time profiles of association with T5 CLPs (0 to 200 s) and of dissociation (200 to 750 s) using pb10 chimeras at increasing concentrations: 0.25, 0.5, 1.0, 2.0 and 4.0 nM for pb10-mC (**c**); 0.3, 0.6, 1.25, 2.5 nM for pb10-Ova (**d**). SPR response is expressed as the percentage of occupied binding-sites on the CLP, in order to cope with the mass difference of the pb10 chimeras. Note that association curves plateau at about 80% of occupied sites. This partial occupancy can be explained by the inaccessibility of some binding sites due to capsid capture on the sensor chip by anti-capsid polyclonal antibodies (see Methods section). Below the graphs are the association and dissociation rate constants k_{on} and k_{off} calculated from the SPR profiles and the resulting dissociation equilibrium constants (K_D). The fitting method used for the determination of these constants is described in the Methods section, according to ref. [20]. **e** Binding assays of pb10 and chimeras to T5 CLPs analyzed by native agarose gel electrophoresis. The [pb10]/[binding site] molar ratio indicated above each lane was calculated as described in the Methods.

with the capsid[20]. These properties suggest that pC could be swapped for a heterologous protein while keeping the interaction of pN with the capsid. Capsids of dsDNA bacteriophages initially assemble into compact procapsids, which undergo expansion upon genome packaging. This structural rearrangement of capsid protein subunits yields mature particles capable of withstanding the internal pressure generated by the packed dsDNA. T5 constitutes a particularly attractive system as stable empty capsids devoid of viral DNA and of decoration protein can be purified from bacteria infected with a T5 phage mutant impaired in DNA packaging. These empty capsids can be matured in their stable expanded conformation and decorated in vitro with pb10[20,21]. Based on the properties of these T5 capsid-like particles (CLPs), we evaluated here their potential as multivalent vaccine platforms. Chimeric proteins composed of pb10 fused to the model Ag ovalbumin (Ova) were shown to retain high-affinity for T5 capsid, thus allowing the self-assembly of a nanoparticle displaying numerous Ag copies. Immunization of mice injected with these nanoparticles elicited robust humoral and cellular immune responses, compared to immunization with the chimeric protein alone. Our results establish the potency of T5-derived CLPs to serve as a vaccination platform without the need for extrinsic adjuvant.

RESULTS

Protein anchoring onto bacteriophage T5 CLPs with picomolar affinity

To assess the potential of T5 CLPs as a protein display nanoparticle, we took advantage of the anchoring domain pN of the decoration protein pb10 (Fig. 1a)[20]. We engineered chimeric proteins formed of full-length pb10 (p) or its pN domain alone fused at their C-terminal end with a heterologous protein: either the fluorescent protein mCherry (mC, 26.8 kDa) yielding pmC and pNmC chimeras or the model Ag Ova (42.8 kDa) to form pO and pNO chimeras (Fig. 1b). One additional construct pCO, formed of pC domain fused to Ova, was used as a negative control for capsid decoration, as pC domain does not bind to T5 capsid[20]. The expression of all fusion genes in E. coli yielded soluble monomeric proteins that were purified successively by affinity, ion exchange and size exclusion chromatography as detailed in the Methods section. Protein purity was assessed by SDS-PAGE analysis (Supplementary Fig. 1). Binding of pb10 chimeras to T5 CLPs was first assessed by Surface Plasmon Resonance (SPR). T5 CLPs were non-covalently captured on a SPR sensor chip through anti-capsid antibodies as previously described[20], and then association and dissociation of pmC, pNmC, pO and pNO were monitored at protein concentrations ranging from 0.25 to 2.5 or 4.0 nM. The SPR real-time profiles of association (200 s) and dissociation (600 s) of pb10 and its chimeras are shown in Fig. 1c, d. As observed for the control protein pb10, association of pmC and pNmC (Fig. 1c) or of pO and pNO (Fig. 1d) with T5 CLPs is fast, while dissociation is remarkably slow, suggesting a quasi-irreversible binding. From the determination of the association and dissociation rate constants k_{on} and k_{off} we calculated the equilibrium dissociation constants (K_D) of $0.9–2.3 \times 10^{-12}$ M for the chimeric proteins, very comparable to pb10 K_D ($1.5–2.3 \times 10^{-12}$ M). These values demonstrate that modification of the C-terminus of pb10 does not alter the picomolar affinity of the pN domain for the capsid, opening the possibility of modifying the pC domain without affecting the capsid decoration process. Binding of each pb10 chimera to T5 CLPs was also assessed by mobility shift assays in native agarose gel electrophoresis (Fig. 1e). CLPs appeared fully decorated with pmC, pNmC, pO and pNO proteins for a [protein]/[binding site] molar ratio in the range 1–1.5, as observed for unmodified pb10, attesting that the pN domain retains its high affinity for T5 CLP during electrophoresis, regardless of the protein linked to its C-terminal end. As expected, pCO protein did not modify T5 CLP

mobility, showing that the fusion of pC with Ova Ag does not lead to unspecific binding to T5 CLP. The successful decoration of CLPs with chimeras formed of two different proteins, mCherry and ovalbumin, suggests that pb10 or pN can accommodate fusion with Ags of different sizes while maintaining their ability to irreversibly bind capsids.

We checked the integrity and Ag load of the CLPs associated with pNO by cryo-electron microscopy (cryo-EM) coupled to image analysis. Representative images of T5 CLPs decorated with pNO are shown in Fig. 2a. Some globular extra densities are visible and decorating the surface of the capsid. They become more visible in the three-dimensional reconstruction obtained from the images. As observed for the wild-type T5 capsid structure decorated with native pb10[19] (EMD-6OMC) (Fig. 1a) the pN domain is visible at low and medium contour levels (Fig. 2b, c, left, middle). Density levels of the pN domain are comparable to those of the capsid protein confirming that all of the pb10 binding sites are occupied. In contrast to the wild-type T5 capsid structure, for which the pC domain of pb10 is too small and too flexible to be rendered (Fig. 1a and ref. [19]), increasing the contour level for the CLP decorated with pNO revealed some smeared densities on top of pN (Fig. 2b, c, right). These densities can without any doubt be attributed to Ova. The fact that Ova is fuzzy is due to the flexibility of the linker between pN and Ova, a behavior also observed for Ags bound on the ADDOMER particle[22]. Together with the previous biochemical and kinetic analysis, cryo-EM data attests for the complete and high affinity decoration of T5 capsids with pb10 chimeras.

Humoral immune responses induced by CLP-bound pb10-Ova chimeras

Seeking to harness T5 capsid as a vaccination platform, we investigated whether anchoring of pO or pNO onto T5 CLP could modulate their immunogenicity following their administration to mice. We first checked that the endotoxin content of pb10-Ova chimeric proteins (pO and pNO) and CLP samples was in the range (20 to 200 EU/mL) acceptable for vaccine formulation[23] (Supplementary Table 1). Then, C57BL/6 mice were subcutaneously injected with pO- or pNO-decorated CLPs or with pO or pNO proteins mixed or not with complete Freund adjuvant (CFA). Sera were collected every two weeks after administration and anti-Ova antibodies (Abs) were quantified by ELISA (Fig. 3). The level of anti-Ova Ab (IgG) was 1000-fold higher in mice injected with either CLP-bound pb10-Ova chimeras than in mice injected with pO or pNO proteins alone. This higher titer in anti-Ova Abs was observed as soon as 14 days post-injection (p.i.) and was maintained up to 6 months (192 days p.i.). Of note, this stronger humoral immune response was observed for both pO- and pNO-CLP, suggesting that the pC domain does not impact the production of anti-Ova Abs. Remarkably, the levels of anti-Ova Abs were similar in mice injected with pO- or pNO-CLP and in mice injected with pO mixed with CFA, a compound well-known for its adjuvant properties[24]. In order to assess the nature of anti-Ova Ab responses, we identified IgG subtypes produced at the peak of the response (day 42 p.i., Fig. 4). A strong production of anti-Ova Abs ($p < 0.001$ compared to mice injected with pO or pNO alone) was observed for all IgG subtypes analysed (IgG1, IgG2b, IgG2c and IgG3) in mice injected with CLP-bound pO or pNO. The comparison with mice injected with pO supplemented with CFA uncovered a bias towards a lower production of IgG1 ($p < 0.001$) and a higher production of IgG3 ($p < 0.05$).

These data show that the binding of multiple copies of pb10-Ova chimeras to T5 CLP elicits strong and long-lasting anti-Ova humoral responses, involving a large panel of IgG subtypes. Furthermore, since no specific adjuvant was added in the vaccine preparation, our results suggest that T5 capsid per se provides an adjuvant effect and influences the nature of Ova-specific Ab responses.
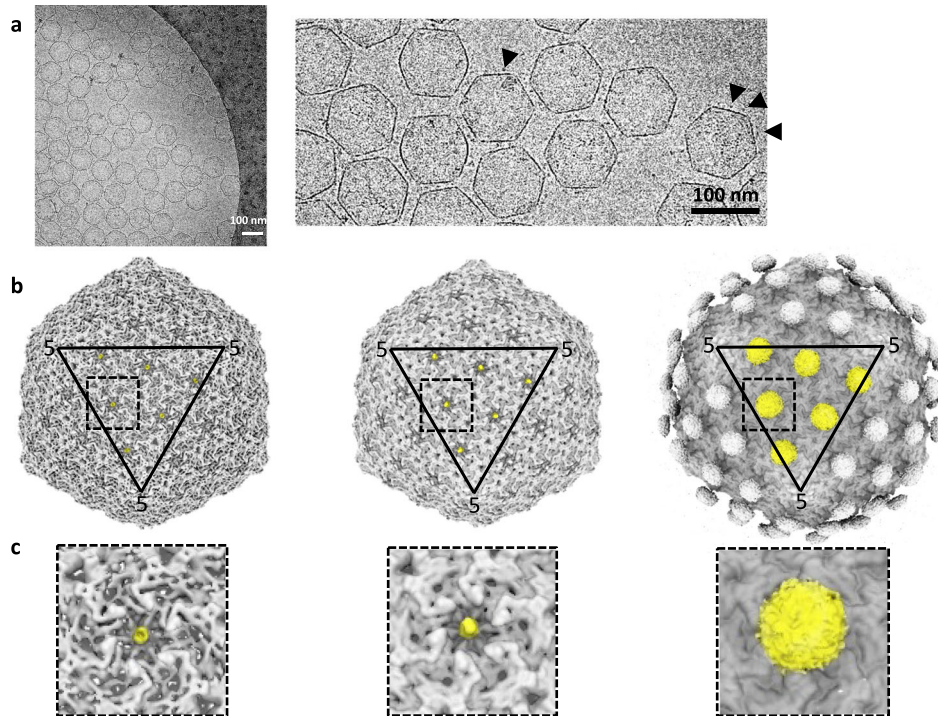
Fig. 2 Cryo-EM image analysis and three-dimensional reconstruction of T5 CLPs decorated with pNO. a Representative example of a cryo-electron microscopy image (left) and enlarged view (right). The arrowheads indicate the presence of Ova at the surface of the CLPs. The scale bars represent 100 nm. **b** Isosurface representation of the 3D structure of T5 CLP decorated with pNO at low (left), medium (middle) and high (right) contour levels. One facet is highlighted by a triangle, the number 5 indicates CP pentamers at the vertices. **c** Enlarged views of the different squares highlighted in b and centered on a CP hexamer. Left: low contour level isosurface representation of pNO 3D structure. Even at low contour level the pN domain is visible (highlighted in yellow) showing that pNO occupies nearly if not 100% of the available sites in the center of hexamers. Middle: medium contour level isosurface representation of pNO 3D structure. The pN domain (yellow) is clearly visible. Right: high contour level isosurface representation of pNO 3D structure. On top of each pN domain an extra density becomes visible, which can unambiguously be attributed to Ova. The Ova density is smeared because of the presence of a flexible linker between pN and Ova: different positions of Ova are averaged out in the 3D structure.

Dose-dependent humoral immune responses elicited by CLP-bound pb10-Ova chimeras

To further assess the immunogenicity of the CLP platform, mice were injected twice with different doses of CLP-bound pb10-Ova: low, intermediate and high doses corresponding to 0.1, 1 and 10 µg of pNO grafted onto 0.4, 4.1 and 41 µg of CLP respectively (the molar ratio [pNO]/[CLP binding site] was equal to 1.0 for each dose). A control group of mice was injected with pNO alone at the highest dose. Dose-dependent anti-Ova Ab responses were observed at days 7 and 14 after the first administration with a plateau reached at day 28 (Fig. 5). Although greater variability in anti-Ova Ab responses was observed between mice injected at the lowest dose, anti-Ova Ab titers determined at all time points after the first administration were significantly higher than those observed in mice injected with pNO alone (10 µg). Following the second administration, a boost in anti-Ova Ab responses was observed for mice injected with low and intermediate dose of pNO-CLP but not with the highest one (Supplementary Fig. 2). In parallel to anti-Ova Ab responses, we observed a dose-dependent production of anti-CLP Abs (Supplementary Fig. 3). These data demonstrate that strong Ab responses are (i) elicited by very low doses of CLP-Ag and (ii) boosted upon readministration despite the presence of CLP Abs produced after the first injection.

Anchoring of pb10-Ova chimeras to T5 CLP is key in mounting humoral immune responses

To examine whether the attachment of the chimeric proteins to T5 CLP is mandatory to mount efficient immune responses, we used pNO and pCO chimeras, which are proficient and deficient for

capsid binding, respectively (see Fig. 1). Of note, previous studies demonstrated that no point mutation in the pN domain could be found to abrogate capsid binding. Affinity could be reduced, but not abolished, only when the mutations affected the 3D structure[20]. For this reason, pCO chimera was used as a control to evaluate the immunogenicity of Ova in the absence of capsid binding. C57BL/6 mice were immunized subcutaneously with pNO or pCO either alone, or combined with T5 CLP, or combined with CFA. Sera were collected at different time points. As reported above, the combination of pNO with T5 CLP led to a kinetics of anti-Ova humoral responses very similar to the combination of pNO with CFA and strongly different from pNO alone (Fig. 6a). In sharp contrast, no significant difference in the response was observed whether pCO was injected alone or with T5 CLP as shown by the measurement of total IgG (Fig. 6b) and IgM as well as IgG subtypes (Supplementary Fig. 4). The weak Ab response observed with pCO mixed with capsids (pCO + CLP) did not stem from a lack of pCO immunogenicity since the combination of pCO and CFA triggered strong humoral responses (Fig. 6b and Supplementary Fig. 4). Altogether, these results indicate that binding of pb10-Ova chimeras to T5 CLP plays a key role in eliciting anti-Ova Ab responses. This is probably due to the clustering of up to 120 copies of Ag on the same particle.

Induction of T cell immune responses by CLP-bound pb10-Ova chimeras

In order to assess anti-Ova CD8$^+$ cellular responses elicited by administration of CLP-bound pO or pNO, splenocyte responses were quantified 10 days after boosting. ELISPOT assays showed a
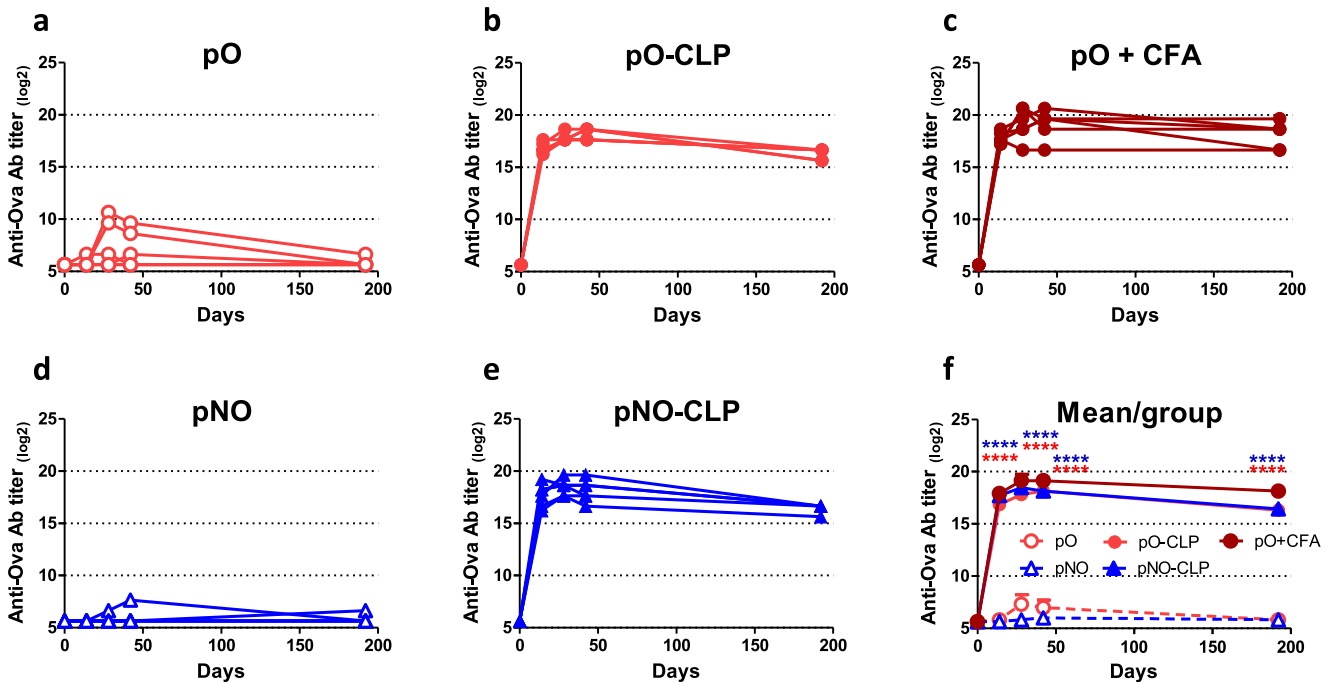
Fig. 3 Kinetics of anti-Ova humoral immune responses elicited by pb10-Ova chimeras. C57BL/6 mice were immunized by a single subcutaneous injection with pb10-Ova chimeras alone (pO or pNO), bound to T5 CLP (pO- CLP or pNO-CLP) or supplemented with CFA (pO + CFA). Titers of Ova-specific IgG were determined by ELISA at different time points after injection. **a–e** Each curve represents titers (log₂ scale) of individual mice ($n = 6$) of the indicated group. **f** Comparison of the kinetics of the different groups (mean + SEM). Titers below 100 were plotted as $\log_2(50)$. Two-way repeated measures ANOVA was used for comparison of responses between groups with and without CLP, at different time points, then Bonferroni post hoc test was used with $p < 0.05$ considered significant. ****$p < 0.0001$ versus pO alone (red) or pNO alone (blue).

high increase in IFNγ-producing CD8⁺ splenocytes in mice injected with pO-CLP or pNO-CLP compared to mice injected with pO or pNO alone (Fig. 7a, $p < 0.001$ and $p < 0.01$, respectively). Moreover, no significant difference was observed between the CD8⁺ cellular responses elicited by pO- and pNO-CLP, suggesting that the pC domain is dispensable. Remarkably, pNO-CLP led to a significantly higher production of IFNγ-producing CD8⁺ T cells and of IFNγ than pNO combined with CFA/IFA (Fig. 7b, c, $p < 0.01$). Thus, in addition to their ability to induce strong humoral responses, T5 CLP displaying multiple copies of pb10-Ova chimeras constituted an efficient tool to trigger CD8⁺ T cell responses.

DISCUSSION

The capsid of bacteriophage T5 offers major advantages for Ag display and vaccination. The procapsid form, devoid of DNA, is easy to produce and to maturate into a capsid-like particle (CLP) with the same structure, stability and affinity for the decoration protein pb10 compared to the native virion[20,21]. In this study, we demonstrated that the fusion of mCherry (25.8 kDa) or ovalbumin (42.8 kDa) to full-length pb10 (18.3 kDa) or to its capsid binding domain pN (8.1 kDa) yielded soluble chimeric proteins retaining picomolar affinity to T5 capsid. Remarkably, this affinity is 1000 fold higher than the nanomolar affinity reported for the other well-known monomeric decoration protein HOC of phage T4, that is used for exposing large Ag on the virion head[25,26]. Such strong affinity ensures the full occupancy of capsid binding sites (120 copies) as evidenced by cryo-electron microscopy data. The easy and regular anchoring of pb10-chimeras onto T5 CLP by mere molecular recognition between pN and CLP is better controlled and more efficient than chemical or bio-conjugation technologies. These remarkable T5 CLP properties are instrumental in achieving

the production of a new nanoparticle displaying large proteins, including Ags of interest.

We probed the vaccine properties of T5 CLPs displaying pb10-Ova chimeric proteins pO or pNO. Their administration to mice elicited long-lasting anti-Ova Ab responses as well as CD8⁺ T cell responses. A single injection of non-adjuvanted CLPs decorated with pO or pNO was sufficient to elicit a strong production of anti-Ova Abs for more than 6 months. Remarkably, these responses were similar to the ones obtained after co-administration of pO or pNO with CFA. The characterization of Ab responses revealed the production of a large panel of IgG subtypes (IgG1, IgG2b, IgG2c and IgG3). This suggests the capacity of Ag-decorated T5 CLP to mobilize different subpopulations of helper or/and follicular helper T cells (Th/Tfh) able to promote B cell differentiation. The production of different IgG subtypes is of major interest to activate different Ab effector functions such as neutralization, phagocytosis, complement activation and cell cytotoxicity[27]. Such large isotypic responses were not reported previously upon vaccination using bacteriophage particles, neither with the infectious bacteriophage T4 displaying Ags from *Yersinia pestis*[28] nor with PP7-derived VLP displaying HPV epitopes[29].

The dose-response study showed that 0.4 μg of T5 CLP displaying 0.1 μg of pNO chimera triggered a higher level of anti-Ova Abs than 10 μg of pNO alone. While further investigations will help to better define the minimum dose of decorated CLPs needed to elicit Ab responses, these results demonstrate that decorated CLPs act in a dose range comparable to the one reported for conjugate protein vaccines[30] or AP205 VLPs conjugated to the SARS-CoV-2 spike protein receptor-binding domain[31].

In the dose-response study, we observed that a second administration of pNO-CLP boosted Ova Ab responses at low and intermediate doses but not at the highest dose. This is probably due to the strong level of Ab response already reached after priming with the highest dose. Interestingly, the increase in
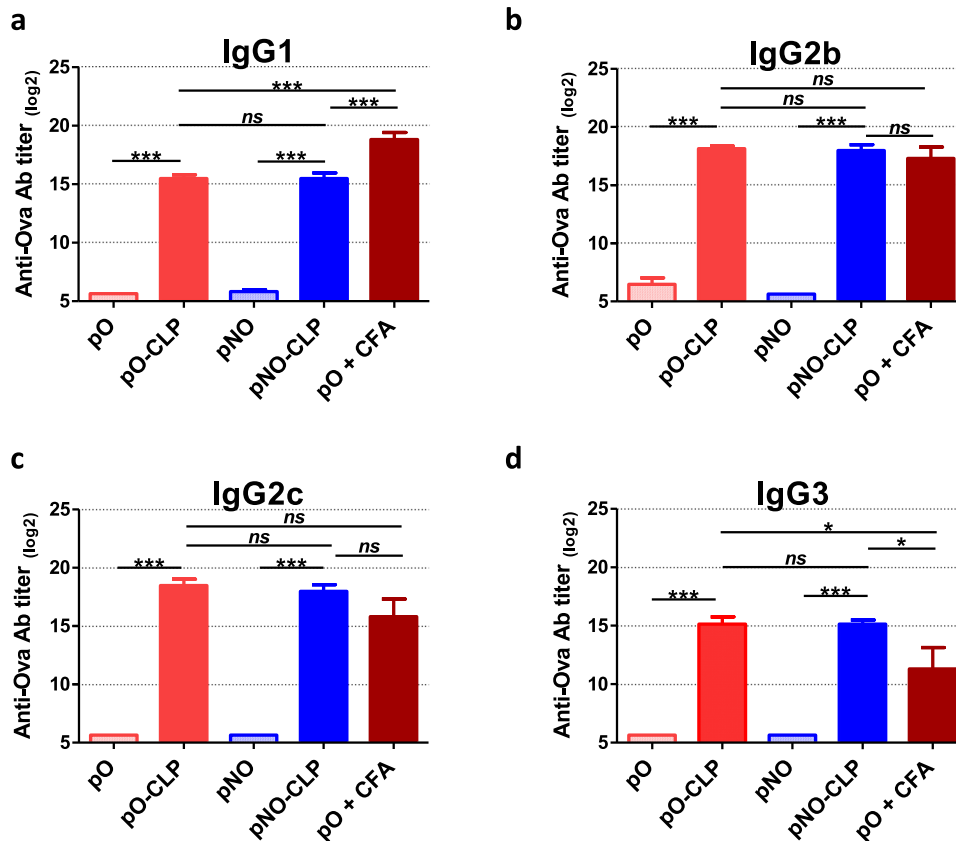
Fig. 4 Nature of the anti-Ova humoral immune responses elicited by pb10-Ova chimeras. Mice were immunized subcutaneously by a single injection of pb10-Ova chimeras alone (pO or pNO), bound to T5 CLP (pO-CLP or pNO- CLP) or supplemented with CFA (pO + CFA). Titers of anti-Ova Abs of IgG1 (**a**), IgG2b (**b**), IgG2c (**c**) and IgG3 (**d**) subtypes were determined by ELISA at day 42 p.i. The results correspond to the mean + SEM of each group ($n = 6$, $\log_2$ scale). Titers below 100 were plotted as $\log_2(50)$. Results were analyzed using one-way ANOVA followed by Tukey's multiple comparison test with $p < 0.05$ considered significant (ns, non-significant; *$p < 0.05$; ***$p < 0.001$).

Ab responses observed at low and intermediates doses suggests that Abs produced after priming does not preclude boosting of Ova Ab responses. The prime-boost was performed with an interval of only 35 days between the two immunizations. However, a longer interval might be necessary to fully differentiate memory B cells and memory follicular helper T cell, to allow their activation upon boosting[32,33].

Beside the humoral responses, we demonstrated that CLPs displaying pb10-Ova proteins elicited a strong induction of CD8^{+} T cell responses. It is likely that this response arose from cross-presentation of Ova Ag following uptake of decorated CLPs by antigen-presenting cells as previously reported for other VLPs[34]. In previous studies, Pouyenfard et al. reported that T7 bacteriophages displaying a CD8^{+} T cell epitope derived from a tumor Ag were able to trigger potent anti-epitope T cell responses. Also, T4 bacteriophage heads (capsids filled with viral DNA) displaying an Ag from *Y. pestis* were shown to induce CD8^{+} T cell responses[8]. To the best of our knowledge, this study is the first to report induction of both humoral and cellular responses by a fully-decorated capsid shell devoid of viral DNA.

Vaccination studies using infectious bacteriophages (Lambda[35,36], PP7[29], T4[28] or T7[37]) or phage heads (Qβ[38] or T4[8] containing RNA or DNA, respectively) reported the induction of immune responses in the absence of adjuvant. Similarly, complexes between T5 CLP and pb10-Ova chimeras triggered potent humoral and cellular responses in absence of any extrinsic adjuvant. As T5 CLP preparations contain low amounts of endotoxin, our results suggest that T5 capsid shell alone, in the absence of phage genome,

provides the adjuvant effect required for efficient vaccination. We speculate that the capsid itself or some structural motifs might be detected by Ag-presenting cells as previously documented for different viruses[39–41]. The strong immunogenicity of T5 CLPs may stem also from the highly ordered and repetitive distribution of Ags (120 copies), which is known to promote the engagement of several B cell receptors at the surface of Ag-specific B cells[1,42]. This immunogenicity might also be favored by the delivery of Ag-CLP complexes to B cell follicles within secondary lymphoid organs, as reported for VLPs derived from other bacteriophages[43].

This study paves the way for the development of T5 CLP-based nanoparticles as a new platform for Ag delivery. Their attractiveness relies on several key features: (i) the tremendous thermal stability of T5 CLPs, which resists temperatures up to 95 °C[21]; (ii) the easiness and low-cost of their large scale production in *E. coli* cells; (iii) the intrinsic adjuvant properties of T5 CLPs, (iv) the capacity of the decoration protein pb10 or its pN domain alone to tolerate the fusion with large size Ags and finally (v) the well-controlled and highly efficient anchoring of a high copy number of the displayed Ag. *Escherichia coli* remains a robust and scalable expression system for the production of CLP and of pN-Ag chimeras including diverse vaccine Ags. However, one major hurdle could arise with Ag that are naturally synthetized with post-translational modifications in eukaryotic cells, and that could be misfolded in bacteria. While we can expect that pN-Ag with disulfide-bonded Ag will be efficiently produced in engineered *E. coli* strains[44,45], other fusion proteins including Ags with glycosylation will require a eukaryotic expression system. Further
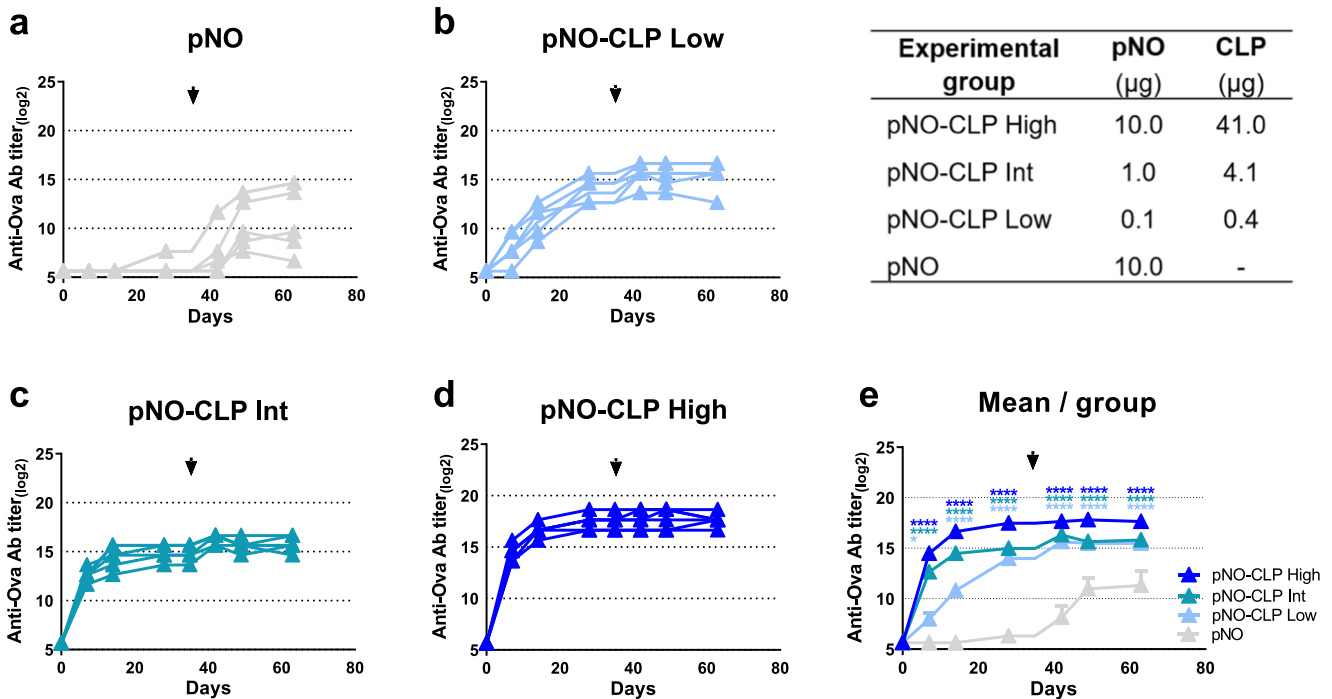
Fig. 5 Dose-dependent anti-Ova humoral immune responses elicited by pb10-Ova chimeras. C57BL/6 mice were immunized twice subcutaneously with pNO alone (10 µg) or with different concentrations of pNO-CLP (low, intermediate and high dose, at 0.1 µg pNO + 0.4 µg CLP (low), 1 µg pNO + 4.1 µg CLP (int), and 10 µg pNO + 41 µg CLP (high). Day 0 and day 35 (arrow) correspond to the first and second injections, respectively. Titers of Ova-specific IgG were determined by ELISA at different time points after injection. Titers below 100 were plotted as $\log_2(50)$. **a–d** Each curve represents titers ($\log_2$ scale) of individual mice ($n = 6$) of the indicated group. **e** Comparison of the kinetics of the different groups (mean + SEM). Two-way repeated measures ANOVA was used for comparison of responses to pNO alone, at different time points, then Bonferroni post hoc test was used with $p < 0.05$ considered significant (ns non-significant; *$p < 0.05$; **$p < 0.01$; ***$p < 0.001$; ****$p < 0.0001$ versus pNO alone). These data are representative of two dose-response studies.
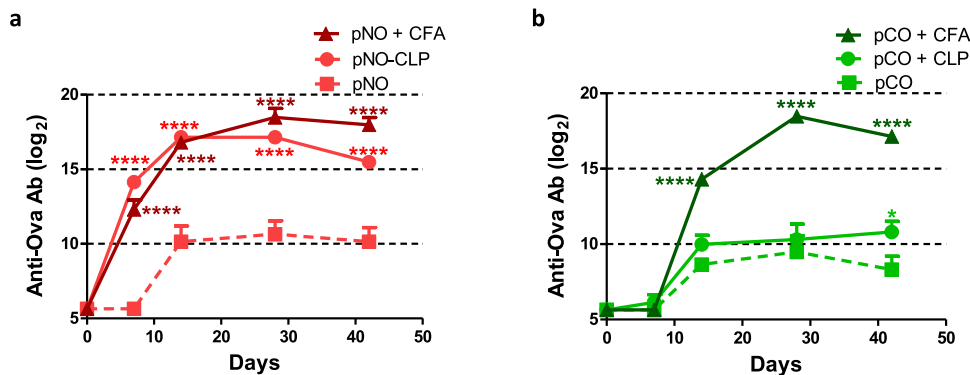

Fig. 6 Kinetics of anti-Ova humoral immune responses elicited by Ova fused to pN or pC domains of pb10. C57BL/6 mice were immunized subcutaneously by a single injection of pb10-Ova chimeras (**a** pNO; **b** pCO) alone or combined with either T5 CLP (pNO-CLP, pCO + CLP) or CFA (pNO + CFA, pCO + CFA). Titers of Ova-specific IgGs were determined by ELISA at different time points after injection. The results correspond to means + SEM of data of individual mice ($n = 6$, $\log_2$ scale). Titers below 100 were plotted as $\log_2(50)$. Two-way repeated measures ANOVA was used for comparison of responses to pNO or pCO, at different time points, then Bonferroni post hoc test was used with $p < 0.05$ considered significant (*$p < 0.05$ and ****$p < 0.0001$ versus pNO or pCO alone).

investigations in these fields will establish the potential of the CLP platform to protect against different types of pathogens.

METHODS
Expression vectors for the production of pb10-mCherry and pb10-Ovalbumin chimeras
The coding sequence of the full-length decoration protein pb10 (GenBank accession number: AAU05286) was previously cloned

into the pET28b vector in frame with a C-terminal His-Tag[20]. The gene encoding variants of pb10 fused in their C-terminal end with mCherry (Red fluorescent protein, GenBank accession number AAV52164) or Ova (Ovalbumin, GenBank accession number J00895) were cloned in pET28b: (i) full-length pb10 for pmC and pO, (ii) the N-terminal capsid binding domain of pb10 (pN, first 73 amino-acids) for pNmC or pNO and (iii) the C-terminal domain of pb10 (pC, amino acids 74 to 164) for pCO. All constructs included a His-Tag in frame with the mCherry or Ova C-terminal end.
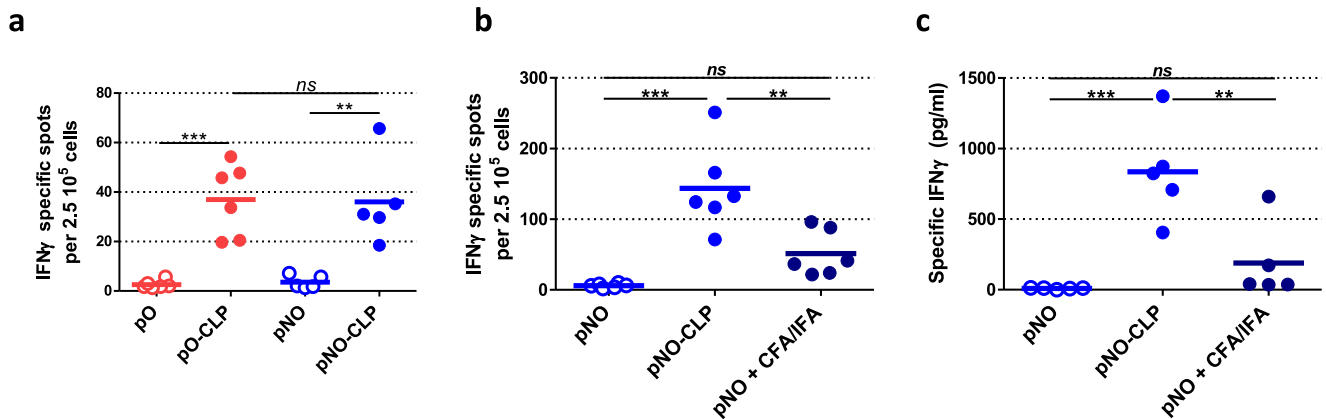
Fig. 7 Cellular immune responses elicited by pb10-Ova chimeras. Mice were immunized (priming) with chimeric proteins either alone (pO, pNO), or bound to T5 CLP (pO-CLP, pNO-CLP) or supplemented with CFA. Mice were subsequently boosted under the same conditions (except that CFA was replaced by incomplete Freund adjuvant, IFA). The interval between priming and boosting was of two (**a**) or six months (**b**). **a**, **b** IFNγ-producing splenocytes were quantified by ELISPOT and (**c**) IFNγ production by splenocytes was measured by ELISA after in vitro restimulation with Ova$_{257-264}$ peptide 10 days after boosting. The bars correspond to the mean of each group ($n = 5$–6) and the circles to results of individual mice. Results were analyzed using one-way ANOVA followed by Tukey's multiple comparison test with $p < 0.05$ considered significant (ns non-significant; **$p < 0.01$; ***$p < 0.001$).

Plasmids pET28-pmC, pET28-pNmC, pET28-pO and pET28-pNO

The expression vectors encoding the fusion proteins were constructed using a ligation independent PCR cloning technology (FastCloning method according to ref. [46] or Quick-Fusion Cloning Kit from Biotool).

For building pb10-mCherry chimeras, the coding sequence of pb10 or its capsid binding domain (pN) were cloned into a pET28b vector encoding mCherry-6His (pET28-mC, a kind gift from Ahmed Bouhss, INSERM U1204, Université Paris-Saclay). The pET28-mC vector was amplified by PCR using a forward primer containing the mCherry gene's first 6 codons and a reverse primer complementary to the NcoI-RBS sequence. The sequences of pb10 or pN inserts were PCR amplified from pET28-pb10 vector[20], using primers including extensions complementary to the ends of pET28-mC PCR product. The two purified amplicons were mixed together according to the FastCloning method[46] before transformation of XL1-Blue competent cells (Agilent Technologies).

For building pO and pNO chimeras, the pET28-pb10[20] vector was amplified by PCR using a forward primer containing the 6His-Tag coding sequence and a reverse primer overlapping the last codons of pb10 sequence (for pO) or the sequence coding the linker that separates the two domains of pb10 (for pNO). The Ova insert coding sequence was PCR amplified from the pcDNA3-OVA plasmid (Addgene). We used a forward primer containing an extension overlapping the last codons of pb10 gene (for pO) or of the linker (for pNO) and a reverse primer extended with the 6His-Tag coding sequence of pET28-pb10 vector. The purified Ova PCR products were mixed with their respective pET28-pb10 PCR products and incubated with the Fusion Enzyme according to the Quick-Fusion Cloning Kit (Biotool) protocol before transformation of XL1-Blue competent cells (Agilent Technologies).

Plasmid pET28-pCO

The fusion of Ova coding sequence with pb10 C-terminal domain (pC) was obtained by means of the Golden Gate cloning method, using type II restriction endonuclease BsaI that cuts DNA outside of its recognition site[47]. We amplified by PCR the two following fragments: (i) the insert sequence encoding the pC-Ova region (pCO) from pET28-pO vector (see above); (ii) the recipient vector pET28b including a 6His sequence to be fused with pCO C-terminal end. For these PCR reactions, we used forward and reverse primers complementary to the region to be amplified at

their 3' end and flanked with a BsaI site at their 5' end, such that digestion of the fragments removes the enzyme recognition sites and generates ends with complementary four nucleotides overhangs.

The cloning step was performed using a one-step restriction-ligation as follows. The amplicons were purified (GeneJet PCR Purification Kit, Thermo Scientific) and 200 ng of each product was added to a mix containing 1U of T4 ligase (Thermo #EL0011), 10 U of BsaI (NEB #R0535), 1 µL DpnI (Thermo #FD1703) in 1X T4 ligase buffer. The mix was incubated for 60 cycles of 37 °C and 22 °C, 5 min each, followed by the final steps at 50 °C for 1 h and 98 °C for 20 min. The assembly reaction was then used for transformation of XL1-Blue competent cells (Agilent Technologies).

The oligonucleotides used for generating the pb10-chimera expression vectors are detailed in Supplementary Table 2. The sequence of each construction was checked by Sanger DNA sequencing.

Production and purification of pb10 chimeric proteins

E. coli BL21 (DE3) cells harboring each of the different pb10 expression vectors were grown in LB medium supplemented with 50 µg/mL kanamycin at 37 °C for pmC, pNmC, and pCO or at 28 °C for pO and pNO (increased solubility). At mid-exponential growth phase (OD$_{600nm} = 0.6$–0.8), protein expression was induced by addition of 0.4 mM isopropyl-β-D-thiogalactopyranoside (IPTG) and the growth continued for 2–3 h. Bacterial cells harvested by centrifugation were suspended in the loading buffer (50 mM Tris-HCl pH 7.4 containing 1 M NaCl), broken by two passages in a French press (10,000 psi) at 4 °C and centrifuged at 4 °C (100,000 g, 30 min). The supernatant was incubated at 4 °C for at least 8 h with 1% n-Octyl-β-d-Glucopyranoside (OG), a detergent used to solubilize contaminant endotoxins (Lipopolysaccharide molecules) originating from *E. coli* outer membranes. It was then loaded onto a 5 mL HisTrap™ FF column (Cytiva) pre-equilibrated in the loading buffer supplemented with 0.2% Lauryldimethylamine-N-oxide (LDAO) and connected to an ÄKTA purifying system. The pb10-mC or -Ova chimeras were eluted with a 0–1 M imidazole gradient in the presence of 0.1% LDAO and the eluted fractions were collected for further purification in the absence of detergent, by cation or anion exchange chromatography, depending on the calculated isoelectric point (pI) of the pb10 fusion proteins. Full-length pb10 (pI = 7.9) was purified on a 5 mL HiTrap SP column (Cytiva) as previously described[20], while pmC (pI = 6.4), pNmC

(pI = 7.0), pO (pI = 6.0), pNO (pI = 6.2) and pCO (pI = 5.4) were purified on a 5 mL HiTrap Q HP column (Cytiva) pre-equilibrated in 50 mM Tris-HCl buffer pH 8.0. The proteins were eluted with a 0–1 M NaCl gradient, concentrated on a centrifugal filter (Amicon® Ultra-4, 10 kD, Millipore) and finally purified by size exclusion chromatography on a Superdex 75 10/300 column (Cytiva) pre-equilibrated in Phosphate-Buffered Saline (PBS). Protein concentrations were determined by measuring the absorbance at 280 nm and using the theoretical extinction coefficients of 22,920 $M^{-1}cm^{-1}$ for pb10, 57,300 $M^{-1}cm^{-1}$ for pmC, 45,840 $M^{-1}cm^{-1}$ for pNmC, 54,320 $M^{-1}cm^{-1}$ for pO and 42,860 $M^{-1}cm^{-1}$ for pNO and pCO determined with the online Expasy ProtParam tool[48].

Production and purification of T5 CLPs
In order to produce phage T5 empty capsids (CLPs) lacking pb10, we constructed the double mutant T5ΔdecstAmN5, by cross-infection of the suppressive *E. coli* strain CR63 with the mutant T5stAmN5 bearing an amber mutation in the terminase gene (production of a non-functional truncated terminase in a non-suppressive strain, thus preventing DNA packaging[18]) and the mutant T5Δdec deleted in the gene encoding the decoration protein pb10 (see ref. [20] for the detailed procedure of mutant screening). T5 CLPs were produced by infection of non-suppressive *E. coli* strain F with the double mutant T5ΔdecstAmN5 and purified as previously described[21] with some modifications in the protocol to remove contaminant endotoxins. Briefly, after precipitation of the bacterial lysate with polyethylene glycol followed by centrifugation in glycerol gradients, the fractions containing T5 empty capsids were incubated for at least 8 h with 1% of OG detergent. Then, a first step of anion-exchange chromatography was performed on HiTrapQ HP column (Cytiva) equilibrated in 50 mM Tris buffer, pH 8.0 containing 200 mM NaCl and 0.2% LDAO. After their elution with a 0–1 M NaCl gradient, the empty capsids were dialyzed against 50 mM Tris buffer, pH 8.0 containing 200 mM NaCl without LDAO and re-injected onto the HiTrapQ HP column for a second step of purification by using the same binding and elution solutions without detergent. Transition of T5 empty capsid from their compact state to their stabilized expanded conformation (CLP) was obtained by dialysis against 50 mM Hepes buffer, pH 7.0, for 24–48 h[21]. CLP samples were finally dialyzed against PBS, concentrated on a centrifugal Amicon® Ultra-4 100 K filter unit (Millipore) and stored at 4 °C. CLP concentration was calculated from the measurement of protein concentration as described previously[20].

Determination of endotoxin content
Endotoxin levels in fusion protein and CLP samples used for in vivo experiments were quantified using the Pierce LAL Chromogenic Endotoxin Quantitation Kit according to manufacturer's instructions (Thermo Fisher Scientific). The results are expressed as endotoxin unit (EU) per ml.

Surface plasmon resonance binding assay
SPR experiments were conducted at 25 °C on a T200 instrument (GE Healthcare) using a CM5 sensor chip functionalized by covalent amine coupling of rabbit polyclonal antibodies (≈ 0.5 mg/mL, dilution 1:50) raised against purified empty T5 capsids as described in ref. [20]. The CLPs (0.2 mg/mL) were captured by injection at 5 μL/min in running buffer (PBS with 0.05% Tween 20 and 1 mg/mL BSA) yielding a capsid density of about 900 RU (Supplementary Fig. 5). Native pb10 or its chimeric forms (diluted in running buffer to 0.25–4 nM) were injected for 200 s at 50 μL/min. Running buffer was then flowed for 550 to 700 s at 50 μL/min to monitor protein dissociation. The functionalized surface was then regenerated by 0.85% phosphoric acid for the next cycle of CLP capture followed by protein association

and dissociation. SPR sensorgrams were corrected for non-specific pb10 binding to the anti-capsid surface and for buffer effect by subtracting both pb10 response on the functionalized surface without CLPs and buffer response on captured CLPs. Kinetic evaluation was performed by fitting the experimental curves to a simple Langmuir model using the Biacore T200 Kinetics Summary Software (version 2.0, GE Healthcare). The percentage of occupied binding sites was calculated by dividing the protein association response expressed in RU by the expected response for total capsid decoration ($R_{100\%}$) determined by the following formula: $R_{100\%} = R_{CLP} * 120 * MW_{protein} / 26,018,181$ (with R_{CLP} being the captured CLP response, 120 the number of pb10 binding sites per CLP, $MW_{protein}$ the molecular weight of the pb10-chimeras and 26,018,181 Da the molecular weight of an empty capsid[49]).

Binding assays assessed by native agarose gel electrophoresis
Purified T5 CLPs were mixed with various amounts of the different pb10 constructs at a final capsid concentration of 10 nM and incubated at 4 °C for 30 min. The samples were loaded on a 1.5% agarose gel in TAMg buffer (40 mM Tris-HCl, 20 mM acetic acid, 1 mM $MgSO_4$, pH 8.1) and migrated at 25 V overnight in a cold room. The capsid bands were stained with Coomassie blue. The molar concentration of binding sites was calculated by multiplying the capsid concentration by 120 sites per capsid.

Cryo-EM, image analyses and 3D reconstruction
A 3.5 μL sample of concentrated pNO-decorated CLPs was applied to negatively glow discharged (25 mA, 40 s) R3.5/1 quantifoil copper grids (Quantifoil Micro Tools). The excess of solution was blotted using a Vitrobot Mark IV (FEI) (20 °C, 100% humidity, 2 s blot time and blot force 1) and subsequently flash-frozen in liquid ethane. Automated data collection was performed on a 200 kV Glacios cryo-TEM microscope (Thermo Fischer Scientific) equipped with a K2 direct electron detector (Gatan) using SerialEM[50]. Coma and astigmatism corrections were also performed using SerialEM. Movies of 40 frames were recorded in counting mode at a 36,000× magnification giving a pixel size of 1.145 Å with defocus ranging from −1.0 to −2.5 μm using a multi-shot scheme (3 × 3 grids of holes without moving the stage). Total exposure dose per movie was 40 e − /Å² and total number of images was 2500.

Movie drift correction and CTF determination were performed with Relion[51]. A total number of 12,000 T5 CLPs were automatically selected into 1024 × 1024 pixels boxes from the best 500 images. These boxes were rescaled to 420 × 420 pixels boxes (pixel size of 2.9 Å) and submitted to 2D classification. After extensive selection and generation of an initial model imposing I4 symmetry, 3D refinement generated a final reconstruction including 10,449 particles with a resolution of 5.8 Å (Fourier Shell = 0.143, not shown).

Mouse immunization
Six-week-old C57BL/6 female mice were purchased from Janvier (Le Genest Saint Isle, France). All mice were conditioned for at least 1 week in our animal facilities before beginning the experiments.

Recombinant fusion proteins (3.8 μM) incubated or not with T5 CLP (32 +/− 3 nM, counting as 3.8 μM of binding sites) were injected subcutaneously over the shoulders (one site) in a volume of 50 μl of phosphate-buffered saline (PBS). For each immunization, the total amount of injected proteins was 41 μg of CLPs, decorated with 11.6 μg or 9.9 μg of pO or pNO, respectively, or mixed with 10.1 μg of pCO. In some experiments, a control group received injection of recombinant fusion proteins (3.8 μM) mixed with complete Freund adjuvant (CFA, Sigma) in 50 μl of PBS. Similar conditions were used when a second injection was performed, except for the control group for which recombinant fusion proteins were mixed with incomplete Freund adjuvant (IFA,

Sigma). In the experiment assessing the dose response, mice were immunized twice with pNO alone (10 µg) or with three different doses of pNO-CLP: low (0.4 µg of CLP decorated with 0.1 µg of pNO), intermediate (4.1 µg of CLP decorated with 1 µg of pNO) and high dose (41 µg pf VLP and 10 µg of pNO). For these experiments, a unique master mix of CLP-bound pNO was prepared at the highest concentration and two 10-fold serial dilutions were carried out to obtain the intermediate and low doses while retaining the same pNO/CLP ratio. Mice were anesthetized with isoflurane and blood samples were collected from the submandibular vein at different time points up to 6 months post-injection. Sera were prepared and analysed for the presence of specific antibodies by ELISA as described below. Mice were euthanized by cervical dislocation and spleens were collected 10 days after the second injection to monitor cellular immune responses.

Ethics statement
All animal experiments were approved (authorization number 19055–2919021108472030 v3) by Ethics Committee No. 26 (officially recognized by the French Ministry of Higher Education and Research) in accordance with the Directive 2010/63/UE from the European Parliament and Council of the European Union and its transposition into French Law.

Measurement of humoral immune responses
After coating 96-well plates (Nunc) with 1 µg ovalbumin (Sigma), serial dilutions of the sera in 5% milk PBS-Tween 0.05% were added. Bound antibodies were detected with peroxidase-conjugated anti-mouse IgM (dilution 1:5000, Southern Biotechnology Associates (SBA) 1020-05), IgG (1:5,000, SBA 1030-05), IgG1 (1:5000, SBA 1070-05), IgG2b (1:5000, SBA 1090-05), IgG2c (1:5000, SBA 1079-05) or IgG3 (1:5000, SBA 1100-05) goat Abs. The peroxidase activity was revealed by incubation with the substrate O-phenylenediamine dihydrochloride (Sigma–Aldrich) for 30 min. The reaction was stopped by addition of 3 N HCl and spectrophotometric readings were performed at 490 nm. Titers were defined as the reciprocal of the highest dilution giving an OD_{490} 2-fold above background values.

Measurement of cellular immune responses
Spleens were crushed in RPMI medium with 5% foetal calf serum and 5×10^{-5} M β-mercaptoethanol, and filtered through a 100 µm cell strainer. After removal of blood cells by ACK Lysing Buffer (Invitrogen), the cells were resuspended and the concentration was adjusted at 2.5×10^6 cells/mL. Then splenocytes were restimulated in different conditions (medium alone, $Ova_{257-264}$ peptide (5 µg/mL)) in a volume of 200 µL for one day (ELISPOT) or three days (ELISA). For ELISPOT, plates were revealed with supplied reagents (murine IFNγ ELISPOT kit, Diaclone) and spots were counted with the ImmunoSpot® S6 FluoroSpot Line Plate Reader (C.T.L.). For ELISA, the supernatants were collected and assayed for the presence of IFN-γ using a murine IFN-γ kit (eBioscience). In both ELISPOT and ELISA, restimulation with ionomycine (1 µM) and PMA (0.1 µM) was used to control the viability of lymphocytes.

Statistical analysis
Data from ELISA experiments (titers) were log_2-transformed before analysis. Two-way repeated measures ANOVA was used for comparison of responses measured for different groups at different time points, then Bonferroni post hoc test was used to compare between groups at each time point. Data obtained from splenocyte restimulation assays were analyzed by a one-way ANOVA followed by Tukey's post-hoc test to compare sets of data. All graphs and statistical tests were performed using GraphPad Prism software. Differences were considered significant when $p < 0.05$.

Reporting summary
Further information on research design is available in the Nature Research Reporting Summary linked to this article.

REFERENCES
1. Bachmann, M. F. & Jennings, G. T. Vaccine delivery: a matter of size, geometry, kinetics and molecular patterns. *Nat. Rev. Immunol.* **10**, 787–796 (2010).
2. Mohsen, M., Gomes, A., Vogel, M. & Bachmann, M. Interaction of viral capsid-derived virus-like particles (VLPs) with the innate immune system. *Vaccines* **6**, 37 (2018).
3. Kelly, H. G., Kent, S. J. & Wheatley, A. K. Immunological basis for enhanced immunity of nanoparticle vaccines. *Expert Rev. Vaccines* **18**, 269–280 (2019).
4. Schiller, J. & Lowy, D. Explanations for the high potency of HPV prophylactic vaccines. *Vaccine* **36**, 4768–4773 (2018).
5. Tornesello, A. L., Tagliamonte, M., Buonaguro, F. M., Tornesello, M. L. & Buonaguro, L. Virus-like particles as preventive and therapeutic cancer vaccines. *Vaccines (Basel)* **10**, 227 (2022).
6. de Vries, C. R. et al. Phages in vaccine design and immunity; mechanisms and mysteries. *Curr. Opin. Biotechnol.* **68**, 160–165 (2021).
7. González-Mora, A., Hernández-Pérez, J., Iqbal, H. M. N., Rito-Palomares, M. & Benavides, J. Bacteriophage-based vaccines: a potent approach for antigen delivery. *Vaccines (Basel)* **8**, E504 (2020).
8. Tao, P. et al. In vitro and in vivo delivery of genes and proteins using the bacteriophage T4 DNA packaging machine. *Proc. Natl Acad. Sci. USA* **110**, 5846–5851 (2013).
9. Zhu, J. et al. A universal bacteriophage T4 nanoparticle platform to design multiplex SARS-CoV-2 vaccine candidates by CRISPR engineering. *Sci. Adv.* **7**, eabh1547 (2021).
10. Fauconnier, A. Phage therapy regulation: from night to dawn. *Viruses* **11**, 352 (2019).
11. Peabody, D. S., Peabody, J., Bradfute, S. B. & Chackerian, B. RNA phage VLP-based vaccine platforms. *Pharmaceuticals (Basel)* **14**, 764 (2021).
12. Pumpens, P. et al. The true story and advantages of RNA phage capsids as nanotools. *Intervirology* **59**, 74–110 (2016).
13. Cielens, I. et al. Mosaic RNA phage VLPs carrying domain III of the West Nile Virus E protein. *Mol. Biotechnol.* **56**, 459–469 (2014).
14. Thrane, S. et al. Bacterial superglue enables easy development of efficient virus-like particle based vaccines. *J. Nanobiotechnol.* **14**, 30 (2016).
15. Fougeroux, C. et al. Capsid-like particles decorated with the SARS-CoV-2 receptor-binding domain elicit strong virus neutralization activity. *Nat. Commun.* **12**, 324 (2021).
16. Chang, J. R. et al. Phage lambda capsids as tunable display nanoparticles. *Biomacromolecules* **15**, 4410–4419 (2014).
17. Davenport, B. J. et al. Phage-like particle vaccines are highly immunogenic and protect against pathogenic coronavirus infection and disease. *npj Vaccines* **7**, 57 (2022).
18. Zivanovic, Y. et al. Insights into bacteriophage T5 structure from analysis of its morphogenesis genes and protein components. *J. Virol.* **88**, 1162–1174 (2014).
19. Huet, A., Duda, R. L., Boulanger, P. & Conway, J. F. Capsid expansion of bacteriophage T5 revealed by high resolution cryoelectron microscopy. *Proc. Natl Acad. Sci. USA* **116**, 21037–21046 (2019).
20. Vernhes, E. et al. High affinity anchoring of the decoration protein pb10 onto the bacteriophage T5 capsid. *Sci. Rep.* **7**, 41662 (2017).
21. Preux, O. et al. A two-state cooperative expansion converts the procapsid shell of bacteriophage T5 into a highly stable capsid isomorphous to the final virion head. *J. Mol. Biol.* **425**, 1999–2014 (2013).
22. Chevillard, C. et al. Elicitation of potent SARS-CoV-2 neutralizing antibody responses through immunization with a versatile adenovirus-inspired multimerization platform. *Mol. Ther.* **30**, 1913–1925 (2022).

23. Brito, L. A. & Singh, M. Acceptable levels of endotoxin in vaccine formulations during preclinical research. *J. Pharm. Sci.* **100**, 34–37 (2011).

24. Bennett, B., Check, I. J., Olsen, M. R. & Hunter, R. L. A comparison of commercially available adjuvants for use in research. *J. Immunol. Methods* **153**, 31–40 (1992).

25. Shivachandra, S. B. et al. Multicomponent anthrax toxin display and delivery using bacteriophage T4. *Vaccine* **25**, 1225–1235 (2007).

26. Fokine, A. et al. Structure and function of Hoc—a novel environment sensing device encoded by T4 and other bacteriophages. *Viruses* **15**, 1517 (2023).

27. Lu, L. L., Suscovich, T. J., Fortune, S. M. & Alter, G. Beyond binding: antibody effector functions in infectious diseases. *Nat. Rev. Immunol.* **18**, 46–61 (2018).

28. Tao, P. et al. Mutated and bacteriophage T4 nanoparticle arrayed F1-V immunogens from Yersinia pestis as next generation plague vaccines. *PLoS Pathog.* **9**, e1003495 (2013).

29. Tumban, E., Peabody, J., Peabody, D. S. & Chackerian, B. A universal virus-like particle-based vaccine for human papillomavirus: longevity of protection and role of endogenous and exogenous adjuvants. *Vaccine* **31**, 4647–4654 (2013).

30. Arunachalam, A. B., Vile, S. & Rosas, A. A mouse immunogenicity model for the evaluation of meningococcal conjugate vaccines. *Front Immunol* **13**, 814088 (2022).

31. Tan, T. K. et al. A COVID-19 vaccine candidate using SpyCatcher multimerization of the SARS-CoV-2 spike protein receptor-binding domain induces potent neutralising antibody responses. *Nat. Commun.* **12**, 542 (2021).

32. Sallusto, F., Lanzavecchia, A., Araki, K. & Ahmed, R. From vaccines to memory and back. *Immunity* **33**, 451–463 (2010).

33. Crotty, S. T. Follicular helper cell biology: a decade of discovery and diseases. *Immunity* **50**, 1132–1148 (2019).

34. Li, W. et al. P22 virus-like particles as an effective antigen delivery nanoplatform for cancer immunotherapy. *Biomaterials* **271**, 120726 (2021).

35. Gamage, L. N. A., Ellis, J. & Hayes, S. Immunogenicity of bacteriophage lambda particles displaying porcine Circovirus 2 (PCV2) capsid protein epitopes. *Vaccine* **27**, 6595–6604 (2009).

36. González-Cano, P. et al. Lambda display phage as a mucosal vaccine delivery vehicle for peptide antigens. *Vaccine* **35**, 7256–7263 (2017).

37. Pouyanfard, S., Bamdad, T., Hashemi, H., Bandehpour, M. & Kazemi, B. Induction of protective anti-CTL Epitope responses against HER-2-positive breast cancer based on multivalent T7 phage nanoparticles. *PLoS One* **7**, e49539 (2012).

38. Khan, F. et al. Head-to-head comparison of soluble vs. Qβ VLP circumsporozoite protein vaccines reveals selective enhancement of NANP repeat responses. *PLoS One* **10**, e0142035 (2015).

39. Shepardson, K. M. et al. Induction of antiviral immune response through recognition of the repeating subunit pattern of viral capsids is toll-like receptor 2 dependent. *mBio* **8**, e01356–17 (2017).

40. Gogokhia, L. et al. Expansion of bacteriophages is linked to aggravated intestinal inflammation and colitis. *Cell Host Microbe* **25**, 285–299.e8 (2019).

41. Hösel, M. et al. Toll-like receptor 2-mediated innate immune response in human nonparenchymal liver cells toward adeno-associated viral vectors. *Hepatology* **55**, 287–297 (2012).

42. Kelly, H. G. et al. Self-assembling influenza nanoparticle vaccines drive extended germinal center activity and memory B cell maturation. *JCI Insight* **5**, e136653 (2020).

43. Link, A. et al. Innate immunity mediates follicular transport of particulate but not soluble protein antigen. *J. Immunol.* **188**, 3724–3733 (2012).

44. Berkmen, M. Production of disulfide-bonded proteins in Escherichia coli. *Protein Expr. Purif.* **82**, 240–251 (2012).

45. Eaglesham, J. B., Garcia, A. & Berkmen, M. Production of antibodies in SHuffle Escherichia coli strains. *Methods Enzymol.* **659**, 105–144 (2021).

46. Li, C. et al. FastCloning: a highly simplified, purification-free, sequence- and ligation-independent PCR cloning method. *BMC Biotechnol.* **11**, 1–10 (2011).

47. Engler, C., Gruetzner, R., Kandzia, R. & Marillonnet, S. Golden gate shuffling: a one-Pot DNA shuffling method based on type IIs restriction enzymes. *PLoS One* **4**, e5553 (2009).

48. Gasteiger, E. et al. Protein identification and analysis tools on the ExPASy server. in *The Proteomics Protocols Handbook* (ed. Walker, J. M.) 571–607 (Humana Press, 2005). https://doi.org/10.1385/1-59259-890-0:571.

49. Dominguez-Medina, S. et al. Neutral mass spectrometry of virus capsids above 100 megadaltons with nanomechanical resonators. *Science* **362**, 918–922 (2018).

50. Schorb, M., Haberbosch, I., Hagen, W. J. H., Schwab, Y. & Mastronarde, D. N. Software tools for automated transmission electron microscopy. *Nat. Methods* **16**, 471–477 (2019).

51. Zivanov, J. et al. New tools for automated high-resolution cryo-EM structure determination in RELION-3. *eLife* **7**, e42166 (2018).

ACKNOWLEDGEMENTS

AUTHOR CONTRIBUTIONS

P.B. and K.B. designed and led the study. E.V. constructed the expression vectors for most pb10-mC and -Ova chimeras, produced and purified the proteins. E.V. and M.R. purified T5 CLPs, performed the decoration assays, and prepared the samples for mice immunization. E.V. and S.H. performed the SPR experiments and analyzed the data with the help of P.E., L.R.-C. and O.R. designed the expression vector for pCO production. N.D. prepared the CLPs decorated with pNO for EM imaging, M.O. performed preliminary negative-stain and cryo-EM imaging to define the best conditions for pNO-CLP reconstructions. G.S. performed capsid imaging on the GLACIOS microscope and 3D reconstruction of pNO-CLP. L.L.C. measured endotoxin content of protein and CLP samples. L.L.C. and C.V. performed mice immunizations, sampled blood and spleen to monitor immune responses using ELISA and ELISPOT. L.L.C., C.V., L.Z., and N.S. performed ELISA experiments. P.B. and K.B. wrote the manuscript with contributions of E.V., O.R. and G.S. All authors reviewed the manuscript.

COMPETING INTERESTS

P.B., E.V., N.D., L.L.C., and K.B. are named as inventors on a patent application filed by the CNRS and University Paris-Saclay based on the presented study (N° PCT/FR2020/051628, WO2021053309).

ADDITIONAL INFORMATION

Supplementary information The online version contains supplementary material available at https://doi.org/10.1038/s41541-023-00798-5.

Correspondence and requests for materials should be addressed to Pascale Boulanger or Karim Benihoud.

Reprints and permission information is available at http://www.nature.com/reprints

Publisher's note Springer Nature remains neutral with regard to jurisdictional claims in published maps and institutional affiliations.